ON THE MECHANICAL AND HYDRAULIC RESPONSE OF SEDIMENTARY ROCKS IN THE PRESENCE OF DISCONTINUITIES

E. Haghighat and S. Pietruszczak [1]

Department of Civil Engineering, McMaster University, Hamilton, Ont., Canada

ABSTRACT

In this study, the mechanical and hydraulic properties of sedimentary rocks are examined. The first part is focused on the analysis of the onset and propagation of damage. The formulation of the problem involves the specification of an anisotropic failure criterion as well as description of inelastic deformation, which includes the time-dependent effects. The discrete propagation of macrocrcaks is simulated using an enhanced constitutive law with embedded discontinuity. The framework is applied to the assessment of long-term damage around a deep-excavation in an anisotropic shale formation. In the second part, the steady state flow in the presence of embedded discontinuities/cracks is addressed by applying a modified form of the Darcy's law. The approach is illustrated by examining the flow pattern in a sedimentary rock sample that contains randomly distributed sealed fractures.

Keywords: Sedimentary rocks, anisotropy, strong discontinuities, constitutive relation, localized deformation

1. Introduction

The assessment of mechanical and hydraulic properties of sedimentary rocks is of a significant interest for a broad range of geo-engineering applications. Among those, perhaps the most critical one is the use of these formations for the geological disposal of nuclear waste. The feasibility of sedimentary rocks, in particular shale/clay, for the disposal concepts has been evaluated in a number of countries (e.g., France, Belgium, Switzerland, etc.) and it has been assessed as a favourable medium for the purpose of the long-term storage. This is primarily due to their adequate

[1] Corresponding author. Tel: +1 (905) 925-9140; Ext: 24007; E-mail address: pietrusz@mcmaster.ca

This paper is dedicated to prof. Tomek Hueckel on the occasion of his 70th birthday

isolation properties, which include low permeability, geological stability and self-healing capacity. However, technical uncertainties about the safety of using geological repositories for the final isolation of high and/or intermediate level nuclear waste still remain unresolved. In particular, the issues related to the assessment of the effects of repository construction and burial of thermally hot wastes on the host rock are still poorly understood. This presents a major concern, as the geologic behavior of the repository area must be predicted over time spans of hundreds of thousands of years. This assessment should include not only the mechanical response, but also the mechanisms of groundwater flow into and radionuclide transport out of the repository.

The mechanical properties of shales are strongly influenced by their microstructure. At both the micro and meso scales, the material displays an inherent anisotropy. In the former case, the texture consists of mineral particles (mostly flakes of clay minerals) which have a preferred orientation due to the sedimentation process. At a mesoscale, there are distinguishable bedding planes marking the limits of strata that can be clearly seen by a visual inspection. The anisotropy has a profound effect on both the strength and deformation properties, which has been documented by a large number of experimental studies. The strength in the compression regime is usually assessed based on the results of triaxial tests that are conducted at different orientation of the bedding planes (cf.[1–6]). The results generally indicate that the maximum strength is associated with specimens in which the direction of major principal stress is either parallel or perpendicular to the bedding planes, while the minimum strength has been observed for orientations between 30 and 60 degrees. The failure mode evolves with the confining pressure. At high pressures, the response is ductile and significant irreversible deformations develop. At low confinement, the unstable strain softening behaviour, associated with brittle failure, takes place. The tensile properties are typically assessed from the results of Brazilian indirect tensile tests. In general, the strength for tension perpendicular to the bedding planes is significantly lower than that for tension along the bedding planes [7,8]. There is also a strong experimental evidence that the behaviour of shale is time-dependent and the effect of creep is significant (e.g.[9,10]). The quantitative aspects are, once more, influenced by the orientation of the bedding planes and at higher deviatoric stress intensities a prolonged period of creep might cause a spontaneous failure of the material.

The hydraulic properties of shales are also affected by the microstructure. The shale matrix contains both the micropores (pores less than 2 nm diameter) and mesopores (pores with 2–50 nm diameter). The smaller pores in the matrix are mainly associated with clay minerals and organic matter. Clay minerals account for about 50-60 wt.% of most shales. As a result of this type of microstructure, the hydraulic conductivity of shale is very low and remains within the range of 10^{-13} - 10^{-9} m/sec. The conductivity in the direction parallel to the bedding planes is typically around 10^{-14} - 10^{-12} m/sec, while that in the direction normal to it is within the range of 10^{-15} - 10^{-13} m/sec. The porosity of shale is 1-10%.

Over the last few decades, an extensive research effort has been devoted to modeling of the mechanical behaviour of anisotropic rocks. A comprehensive review on this topic, examining different approaches, is provided for example in refs. [11,12]. Some further details on the attempts to assess the conditions at failure and on the existing approaches for dealing with description of damage propagation are provided in ref.[13]. This paper is an extension of research recently reported in ref.[13]. Its primary objective is to outline a methodology for assessing the long-term damage in the host rock due to a deep geological excavation. In addition, the issue of the description of hydraulic properties of sedimentary rocks in the presence of discontinuities is also addressed. The paper is organized in the following sequence. In the next section, the general formulation of the constitutive relations governing the homogeneous as well as the localized deformation mode is outlined. This includes the specification of an anisotropic failure criterion as well as a description of both the instantaneous and time-dependent inelastic deformation. The discrete propagation of damage is simulated using an enhanced constitutive law with embedded discontinuity. The framework is then applied to the numerical analysis of a borehole excavation problem and the assessment of the evolution of the excavation damage zone (EDZ). In Section 3, the steady state flow in the presence of embedded discontinuities/cracks is addressed by invoking a modified form of the Darcy's law. The approach is illustrated by examining the flow pattern in a constant head permeability test conducted on a sedimentary rock sample that contains randomly distributed sealed fractures. The paper ends by providing some final remarks.

2. Analysis of damage induced by a deep excavation in an anisotropic shale formation

In this section, the problem of assessment of damage around a deep geological excavation in a sedimentary rock formation is addressed. The analysis employs constitutive relations that describe both the homogeneous deformation mode, associated with anisotropic response, as well as the localized deformation involving the onset and propagation of macrocracks. Below, the details of the formulation are provided first followed by a discussion on the numerical results.

2.1. Formulation of the problem

The conditions at failure, which are identified here with the onset of formation of macrocracks, are defined by invoking the Mohr-Coulomb criterion with a constraint imposed on the strength in the tensile regime. Thus,

$$F=\max\left(F_1,F_2\right)=0;\quad F_1=\sqrt{3}\bar{\sigma}-\eta_f\, g(\theta)\left(\sigma_m+C\right);\quad F_2=\max_{n_i}\left(\sigma_{ij}n_i n_j-f_t(n_i)\right) \tag{1}$$

where, $\bar{\sigma}=\left(J_2\right)^{1/2}$; $\sigma_m=-\frac{1}{3}I_1$; $\theta=\frac{1}{3}\sin^{-1}\left(\frac{-3\sqrt{3}}{2}\frac{J_3}{\bar{\sigma}^3}\right)$ and

$$g(\theta)=\frac{3-\sin\phi}{2\sqrt{3}\cos\theta-2\sin\theta\sin\phi}\;;\qquad \eta_f=\frac{6\sin\phi}{3-\sin\phi}\;;\qquad C=c\cot\phi \tag{2}$$

In the expressions above, I_1 is the first stress invariant, while J_2, J_3 are the basic invariants of the stress deviator. Moreover, θ is the Lode's angle, ϕ and c are the angle of friction and cohesion, respectively. For the tension cut-off criterion, i.e. the second equation in (1), n_i defines the unit normal to the plane, while f_t is the corresponding tensile strength.

An extension to the case of inherent anisotropy can be accomplished by assuming that the values of the strength parameters (in this case η_f, C and f_t) depend on the relative orientation of principal axes of stress and the microstructure. Note that, in the context of the Mohr-Coulomb criterion (1) , the parameter C is associated with a hydrostatic stress state. The latter is, in fact, invariant with respect to orientation of the sample. Thus, in the compression regime, the effects of anisotropy can be primarily attributed to variation in the strength descriptor η_f. Following the methodology outlined in ref.[13] , the anisotropy function is defined as

$$\eta_f=\hat{\eta}_f\left(1+A_{ij}l_il_j+a_1(A_{ij}l_il_j)^2+a_2(A_{ij}l_il_j)^3+\cdots\right);\qquad C=const. \tag{3}$$

Here, l_i represents a unit vector, referred to as a 'loading direction', whose components are the normalized magnitudes of tractions on planes normal to the principal material axes. The latter are defined by the eigenvectors of the operator A_{ij}, which is a traceless second-order tensor. Note that for materials with strong inherent anisotropy, such as shales, the representation (3) does not require a specific fabric descriptor. This is because the principal material directions are known *a priori* and do not change in the course of deformation. An explicit definition is required only in the context of evolving (i.e. induced) anisotropy.

For failure in the tension regime, it is assumed that the macrocrack forms when the normal component of the traction vector, i.e. $\sigma_{ij}n_in_j$, acting on the localization plane reaches a critical value f_t. The latter is again assumed to be orientation-dependent and is expressed in a general form similar to that of eq.(3), i.e.

$$f_t=\hat{f}_t\left(1+\Omega_{ij}n_in_j+b_1(\Omega_{ij}n_in_j)^2+b_2(\Omega_{ij}n_in_j)^3+\cdots\right) \tag{4}$$

where Ω_{ij} is a symmetric traceless tensor which describes the bias in the spatial distribution of f_t . In this case, the assessment of the value of F_2, viz. eq.(1), requires the solution to a constrained optimization problem. The latter may be solved by, for example, Lagrange multipliers method in which case

$$G = \sigma_{ij} n_i n_j - \hat{f}_t (1 + \Omega_{ij} n_i n_j + b_1 (\Omega_{ij} n_i n_j)^2 + b_2 (\Omega_{ij} n_i n_j)^3 + \cdots) - \lambda_1 (n_i n_i - 1); \quad \frac{\partial G}{\partial n_i} = 0 \qquad (5)$$

Here, the stationary conditions for the components of the derivate of G provide a set of equations defining the orientation of the localization plane. Note that when the higher order terms in eq.(4) are neglected, i.e. $b_1 = b_2 = ... = 0$, the problem reduces to an eigenvalue problem, i.e.

$$(B_{ij} - \lambda \delta_{ij}) n_j = 0; \quad B_{ij} = \sigma_{ij} - \hat{f}_t \, \Omega_{ij} \qquad (6)$$

that can again be solved to specify the direction cosines n_i. Clearly, if $\Omega_{ij} = 0$ then the unit normal to the critical plane will be coaxial with the direction of the maximum tensile stress.

The deformation process, prior to localization, may be described by assuming the yield surface in the form similar to representation (1) and attributing the hardening effects to plastic distortion κ, i.e.

$$f = \sqrt{3}\bar{\sigma} - \vartheta g(\theta)\left(\sigma_m + C\right) = 0; \quad \eta = \eta(\kappa) = \eta_f \frac{\xi \kappa}{A + \kappa}; \quad d\kappa = \left(\frac{2}{3} de_{ij}^p \, de_{ij}^p \right)^{1/2} \qquad (7)$$

where de_{ij}^p is the deviatoric part of the plastic strain rate and A and ξ are material constants. The parameter ξ is introduced here in order to define the transition to localized deformation, which is assumed to occur at $\eta = \eta_f$, which implies that $f = F$. In order to describe a progressive transition from compaction to dilatancy, which is typical for shales, a non-associated flow rule is employed with the plastic potential specified as

$$\psi = \sqrt{3}\bar{\sigma} + \eta_c \, g(\theta)\left(\sigma_m + C\right) \ln \frac{\left(\sigma_m + C\right)}{\sigma_m^0} = 0 \qquad (8)$$

where, η_c is the dilatancy coefficient defined as $\eta_c = \alpha \eta_f$ with α representing a material constant.

The deformation process in shales is, in general, time-dependent. Shale has a very small particle size so that the interstitial spaces are very small. As a result, shale can hold significant amounts of fluids. The presence of fluids triggers the chemical interaction which, in turn, leads to the time-dependent evolution of the mechanical properties of shale. The primary effect of the chemo-mechanical influence of fluid phase is the degradation of strength/deformation properties as a result of reduction of surface free energy and/or the mechanism of subcritical crack growth.

A phenomenological description of creep can be developed within the context of chemo-plasticity [14]. Such a framework incorporates a scalar parameter, ζ, which describes the kinetics of creep. The evolution law can be postulated in a general form

$$\zeta = \zeta(t); \quad \dot{\zeta} = \gamma \left\langle \bar{\zeta} - \zeta \right\rangle \tag{9}$$

where $\zeta \in [0, \bar{\zeta}]$ and $\bar{\zeta} \in [0,1]$ corresponds to the stationary state associated with microstructure equilibrium. Thus, the rate of creep is an explicit function of the 'distance' from this equilibrium state which, in turn, may be affected by the chemical composition of fluids, temperature, etc.

For the plasticity framework employed in this work, the effects of creep maybe embedded in the parameters defining the deformation and strength properties. For the latter, one may postulate

$$A_{ij} = A_{ij}^0 - \alpha_1 \zeta A_{ij}^0 - \alpha_2 \zeta A_{ik}^0 A_{kj}^0; \quad \hat{\eta}_f = \hat{\eta}_f^0 (1 - \alpha_3 \zeta); \quad \hat{f}_t = \hat{f}_f^{\,0} (1 - \alpha_4 \zeta) \tag{10}$$

where α_1 through α_4 are material constants and A_{ij}^0, $\hat{\eta}_f^0$, $\hat{f}_t^{\,0}$ refer to the initial conditions (prior to creep). Note that the representation above implies the material directions do not change in the course of creep. In the elasto-plastic regime, the constitutive relation can be formulated by imposing the consistency condition

$$\dot{f} = \frac{\partial f}{\partial \sigma_{ij}} \dot{\sigma}_{ij} + \frac{\partial f}{\partial \varepsilon_{ij}^p} \dot{\lambda} \frac{\partial \psi}{\partial \sigma_{ij}} + \frac{\partial f}{\partial \eta_f} \frac{\partial \eta_f}{\partial \zeta} \dot{\zeta} = 0 \tag{11}$$

Following now the standard plasticity procedure, yields

$$\begin{aligned} &\dot{\varepsilon}_{ij} = C_{ijkl}\, \dot{\sigma}_{kl} + b_{ij} \dot{\zeta}; \\ &b_{ij} = \partial_\zeta C_{ijkl}^e\, \sigma_{kl} + \frac{1}{H} \frac{\partial f}{\partial \zeta} \frac{\partial \psi}{\partial \sigma_{ij}}; \; C_{ijkl} = C_{ijkl}^e + \frac{1}{H} \frac{\partial \psi}{\partial \sigma_{ij}} \frac{\partial f}{\partial \sigma_{kl}}; \quad H = -\frac{\partial f}{\partial \kappa} \frac{\partial \kappa}{\partial \varepsilon_{ij}^p} \frac{\partial \psi}{\partial \sigma_{ij}} \end{aligned} \tag{12}$$

where $C_{ijkl}^e = (D_{ijkl}^e)^{-1}$ is the elastic compliance operator.

The description of localized deformation, involving the onset and propagation of frictional/cohesive macrocracks, is based here on an enhanced form of a constitutive law with embedded discontinuity [15]. Within this approach, a discontinuous motion within a body is expressed in the form

$$v_i(x_\alpha, t) = \hat{v}_i(x_\alpha, t) + \mathcal{H}(\phi) \tilde{v}_i(x_\alpha, t) \tag{13}$$

where $\hat{v}_i$ and $\tilde{v}_i$ are two continuous functions and $\mathcal{H}(\phi)$ is the Heaviside step function. The latter depends on $\phi = \phi(x_i, t)$, which is the level-set function that represents the geometry of the crack. The symmetric part of the gradient operator of (13), denoted below by indices within parenthesis, can be expressed as

$$v_{(i,j)}(x_\alpha,t)=\hat{v}_{(i,j)}(x_\alpha,t)+\mathcal{H}(\phi)\tilde{v}_{(i,j)}(x_\alpha,t)+\delta(\phi)(n_i\tilde{v}_j+n_j\tilde{v}_i)/2 \tag{14}$$

where $\delta(\phi)$ is the Dirac delta function and $n_i=\phi_{,i}$ is the normal to the interface. In the expression above, the first two terms describe the motion in the intact part of the reference volume Δv while the third term, that involves the Dirac function, is associated with the localized deformation along the crack. Taking the volume average of the last term and ignoring the variation of this discontinuous motion within a small enough Δv, one obtains

$$\frac{1}{\Delta v}\int_{\Delta v}\delta(\phi)(n_i\tilde{v}_j+n_j\tilde{v}_i)\,d\Omega\approx\chi(n_i\tilde{v}_j+n_j\tilde{v}_i)\;;\qquad \chi=\frac{\Delta a}{\Delta v} \tag{15}$$

so that

$$\dot{\varepsilon}_{ij}=\bar{\dot{\varepsilon}}_{ij}+\tilde{\dot{\varepsilon}}_{ij}=\bar{\dot{\varepsilon}}_{ij}+\chi(n_i\tilde{v}_j+n_j\tilde{v}_i)/2 \tag{16}$$

The strain localization is typically associated with an elastic response of the intact material. Thus, in order to formulate the problem, we can invoke the elastic stiffness operator D^e_{ijkl}, i.e.

$$\dot{\sigma}_{ij}=D^e_{ijkl}(\dot{\varepsilon}_{kl}-\tilde{\dot{\varepsilon}}_{kl})=D^e_{ijkl}\dot{\varepsilon}_{kl}-D^e_{ijkl}(\chi\dot{g}_k n_l) \tag{17}$$

Now, the interfacial constitutive relation has the general form $\dot{t}_i=K_{ij}\dot{g}_j$ where t_i is the traction vector while K_{ij} is the tangential stiffness. By imposing the continuity condition along the interface, i.e. $n_i\dot{\sigma}_{ij}=\dot{t}_j=K_{ji}\dot{g}_i$ one obtains, after some algebraic transformations

$$\dot{\sigma}_{ij}=\tilde{D}_{ijkl}\dot{\varepsilon}_{kl};\quad \tilde{D}_{ijkl}=D^e_{ijkl}-D^e_{ijpq}E_{pqrs}D^e_{rskl};\quad E_{ijpq}=\chi\,n_i(K_{jp}+\chi n_r D^e_{rjps}n_s)^{-1}n_q \tag{18}$$

where $\tilde{D}_{ijkl}$ is the tangential operator. It should be pointed out that, unlike in the smeared representation [16], the discontinuity is defined here at the element level, not at individual Gauss points, and it's traced by the level-set method. In this way, the discrete nature of the damage propagation process can be modeled.

2.2 Numerical analysis

The constitutive relations described in the preceding section incorporate material functions/parameters that need to be identified from a suitable experimental program. A general procedure for specification of constants embedded within the framework employing the anisotropy parameter(s) is discussed in details in refs.[13,17]. The numerical example given here is related to the assessment of EDZ around a circular borehole excavated in an anisotropic shale formation. The selected material properties are representative of Opalinus Clay from the region of Mont Terri

URL and have been estimated based on the information provided in ref.[18]. It should be pointed out that the experimental data provided in [18] is rather limited and it's not adequate to identify all parameters employed. However, the other existing sources of data, e.g.[10,19], are even more restrictive in this respect and the scatter of the experimental results is very high (sometimes in excess of 100%, cf.[10]). Therefore, the focus here is on qualitative, rather than quantitative, assessment of the evolution of EDZ.

The elastic constants were taken as [18]

$$E_1 = 1.3 GPa,\ E_2 = 3.8 GPa,\ \nu_{12} = 0.25,\ n_{22} = 0.35,\ G_{12} = 0.9 GPa$$

where $1, 2$ refer to the normal and tangential directions, respectively, to the rock stratification. The strength parameters, viz. eq.(3), have been estimated by assuming $C = 2.5 MPa$ (which is within the range of values given in ref.[18]) and employing the results of a series of axial compression tests at different orientation of the bedding planes. Fig.1 shows the best-fit quadratic (i.e. $a_2 = a_3 = ... = 0$) approximation to the data plotted in the affined space $\{\eta_f, \beta\}$, where β defines the orientation of the bedding planes with respect to the horizontal axis. Here, the data set includes the results of FEM/DEM simulations as reported in ref.[18], which are plotted together with the range of experimental values. The adjacent figure gives the linear (i.e. $b_2 = b_3 = ... = 0$) approximation to the distribution of tensile strength f_t, viz. eq.(4). The coefficients of both approximations have been identified as

$$\hat{\eta}_f = 0.9922,\ A_2 = 0.321,\ b_1 = 2.001,\ \hat{f}_t = 0.98 MPa,\ \Omega_2 = 0.1939$$

Fig.2 shows the predicted variation of unconfined compressive strength f_c. It is evident here that the key values, corresponding to different orientations β, are consistent with the data provided in ref.[18].

Again, no adequate information is available here for the specification of parameters governing the deformation characteristics in the inelastic range. Given this limitation, some typical values of hardening/ dilatancy constants (cf. ref.[20]), which appear in eqs.(7)-(8), have been selected, viz.

$$A = 0.001,\ \alpha = 0.9,\ \zeta = 1.25$$

Fig.3 shows the numerical predictions of a series of unconfined axial compression tests conducted on samples with different orientation of bedding planes. Note that the simulations are terminated here at the onset of brittle fracture, which is associated with unstable strain softening response, as the latter should be dealt with at the level of a boundary value problem. The details on the

specification of the stiffness operator K_{ij} appearing in eq. (18), together with relevant information on the choice of material parameters, are provided in ref. [13].

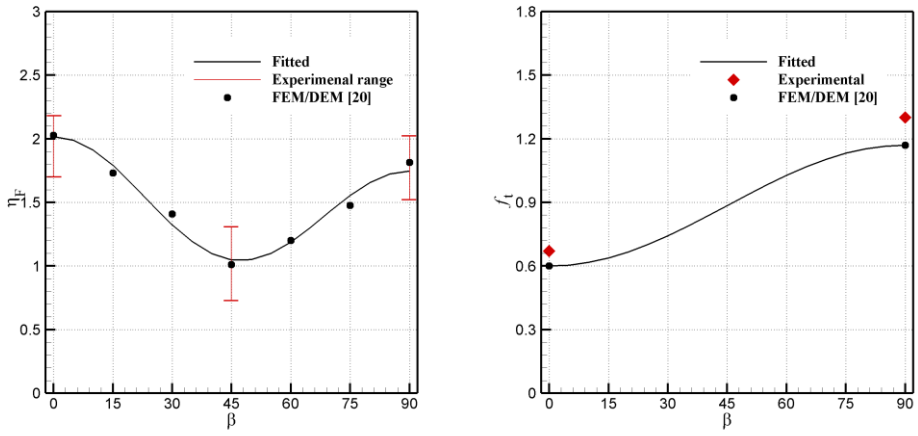

Figure 1- Variation of η_f (left) and f_t (right) with bedding planes orientation β

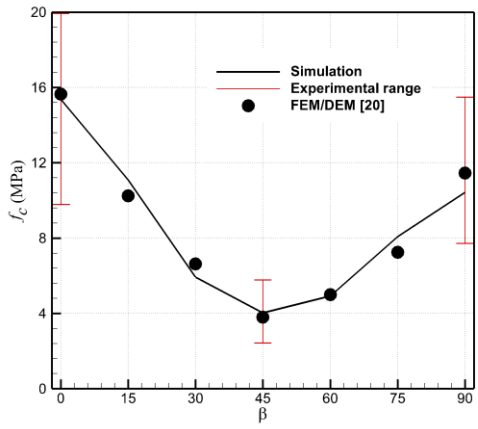

Figure 2- Variation of uniaxial compressive strength f_c with orientation of bedding planes

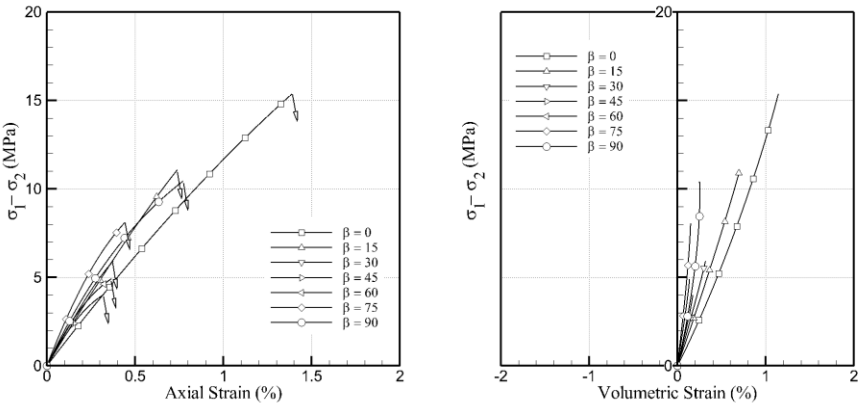

Figure 3- Numerical simulations of unconfined axial compression tests at different orientation of bedding planes

The geometry of the excavation problem and the FE discretization are shown in Fig. 4. The borehole is 1.4m in radius and the initial in-situ stress state was assumed to comprise the vertical stress of 2.5 MPa and the lateral stress of 1.5MPa (cf. ref.[18]). The focus in the analysis was on modelling of long-term damage induced by excavation.

The first stage of the analysis involved the excavation in the intact material. It should be noted that after the excavation is complete, a time-dependent evolution of properties takes place associated with a chemical interaction in the presence of fluid phase. An accurate assessment in this respect requires a description of the creep phenomenon, as described in section 2.1. As mentioned earlier, given the limited experimental information, the focus here is on a qualitative, rather than quantitative, assessment of the evolution of EDZ. Therefore, the creep framework, viz. representation (12), has not been explicitly incorporated here. Instead, the simulation of the onset and propagation of damage near the excavation zone was carried out by degrading the strength parameter $C = 2.5\,MPa$ by 50% to a residual value of $C = 1.25\,MPa$.

The main results of the analysis are presented in Fig.5-8. All simulations have been conducted for two different orientations of bedding planes viz. $\beta = 0^0$ and $\beta = 45^0$. Fig.5 shows the distribution of the ratio η / η_f at three different stages of the simulations, i.e. (a) the end of excavation, (b) the crack initiation, and (c) the end of degradation process. The value of $\eta / \eta_f \to 1$ is indicative of the onset of localized fracture. It is evident here that for the intact properties the behavior remains in the stable regime (i.e., no localization). The macrocracks develop during the degradation stage and the predicted crack pattern is shown in Figs. 5(b) and 5(c). It can be seen from Fig.5 that the extent of damage in case of inclined bedding planes is more severe than that for horizontal stratification. The corresponding plastic distortion and horizontal/vertical displacement contours are shown in Fig 6-8, respectively. It should be mentioned that the solution

presented here is not affected by the FE discretization. This issue was explicitly addressed in ref.[13] in the context of simulations of a series of biaxial compression tests. It was demonstrated that by invoking the constitutive law with embedded discontinuity, which incorporates the characteristic dimension χ, eq.(15), the solution is virtually mesh independent.

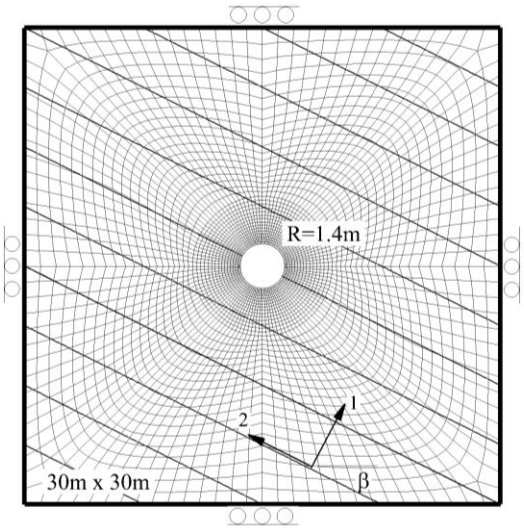

Figure 4- Geometry and FE discretization for the excavation problem

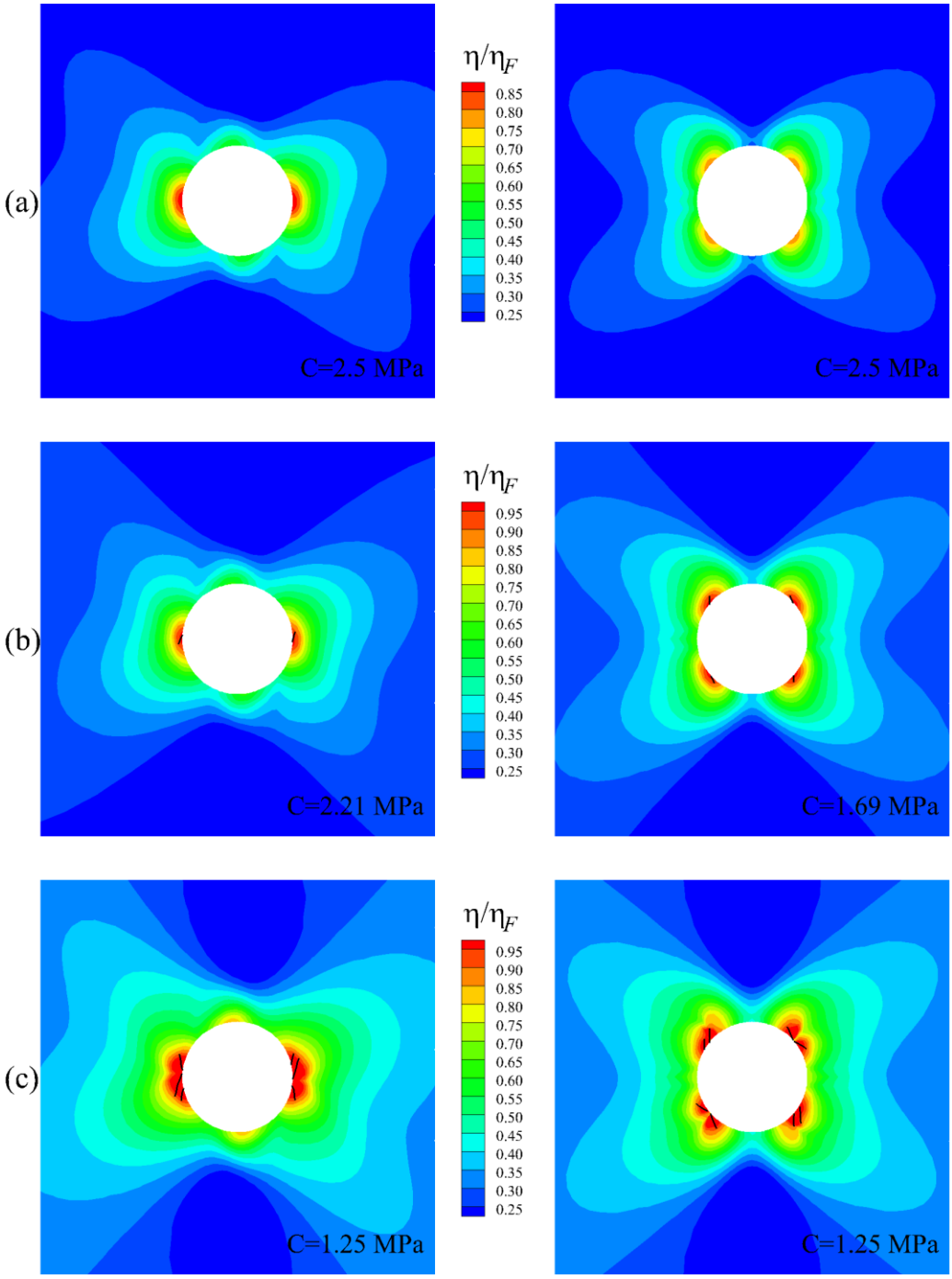

Figure 5- Distribution of η / η_f at (a) end of excavation, (b) crack initiation, and (c) end of analysis. Left : $\beta = 45^0$; Right: $\beta = 0^0$

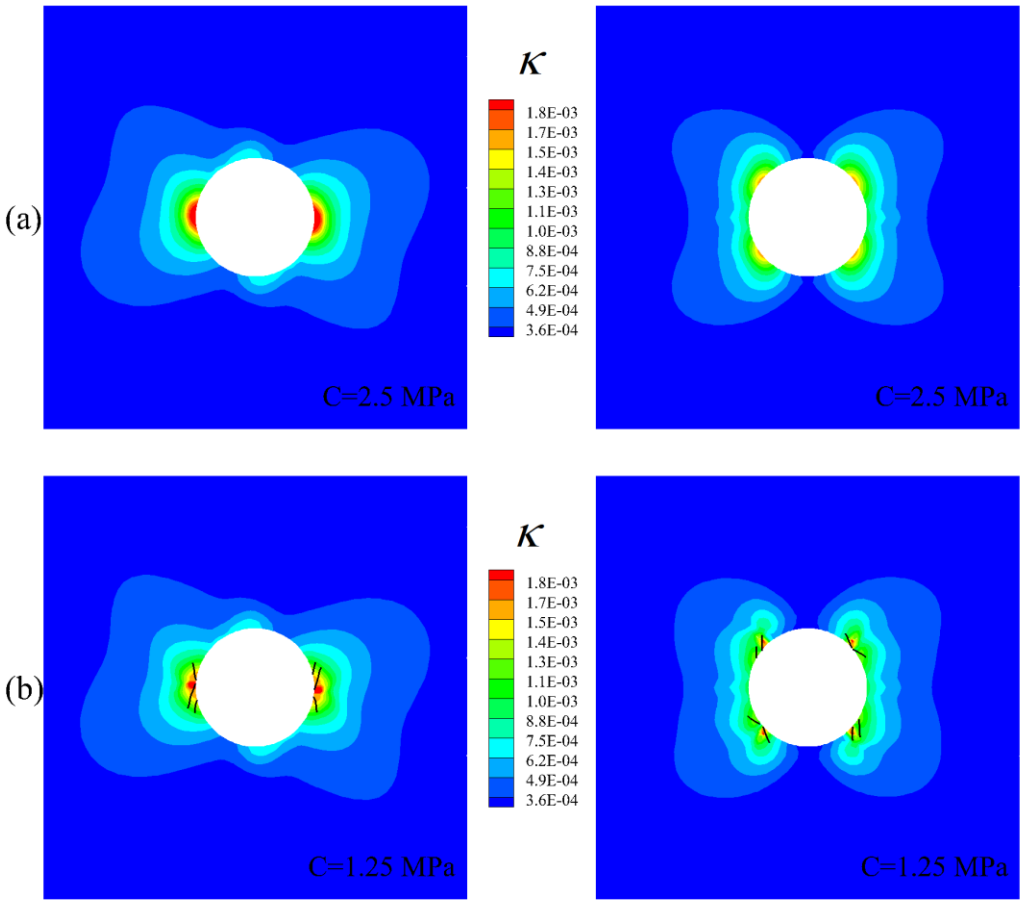

Figure 6- Distribution of plastic distortion κ at (a) end of excavation and (b) end of degradation process. Left : $\beta = 45^0$; Right: $\beta = 0^0$

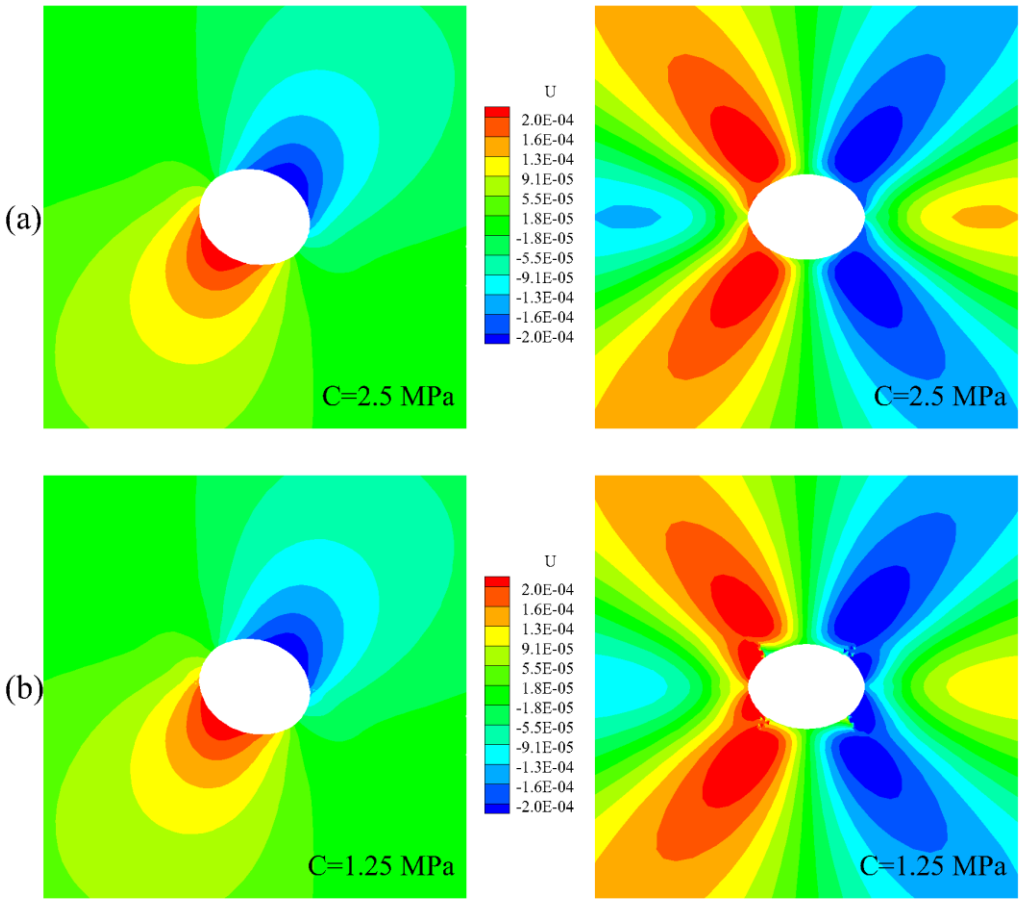

Figure 7- Distribution of horizontal displacement U at (a) end of excavation, (b) end of degradation process. Left : $\beta = 45^0$; Right: $\beta = 0^0$

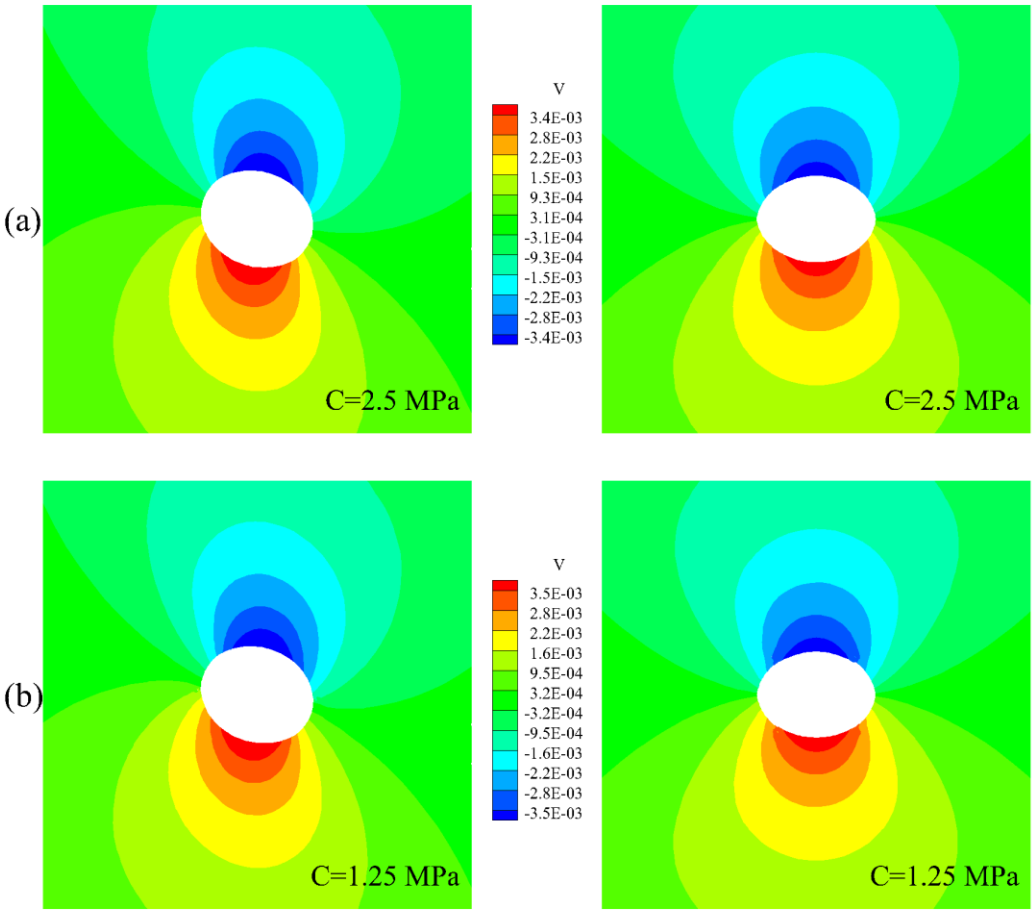

Figure 8- Distribution of vertical displacement V at (a) end of excavation, (b) end of degradation process. Left : $\beta = 45^0$; Right: $\beta = 0^0$

3. Analysis of a steady-state flow in shale formations in the presence of impermeable discontinuities

In this section, a steady state flow in a sedimentary rock that contains discontinuities is examined. Within the considered domain, the total head of energy is assumed to be discontinuous and it's again defined in terms of two independent continuous functions combined with the Heaviside function. Evaluating the gradient operator and averaging over the considered referential volume leads to a discontinuous form of the Darcy's law. The approach is an extension of the Fourier law with embedded discontinuity [21] that is applied here in the context of an anisotropic flow. If the cracks are impermeable (sealed) the condition of zero flux across the interface provides an expression for an equivalent discontinuous hydraulic conductivity/permeability operator. The

formulation is illustrated by conducting a finite element analysis that involves a steady state flow around a set of impervious cracks embedded within the flow domain.

3.1. Formulation of the problem

Following the approach similar to that employed in the previous section, viz. eqs.(13)-(15), one can arrive at a simple and efficient way of defining the flow properties in the domain adjacent to an impermeable interface. For this purpose, consider a discontinuous scalar field variable φ

$$\varphi = \hat{\varphi} + \mathcal{H}\tilde{\varphi} \rightarrow \varphi_{,i} = \hat{\varphi}_{,i} + \mathcal{H}\tilde{\varphi}_{,i} + \delta_{\Gamma}\tilde{\varphi}n_i \tag{19}$$

where $\hat{\varphi}$ and $\tilde{\varphi}$ are two continuous functions and $\mathcal{H} = \mathcal{H}(\phi)$ is the Heaviside function (cf. eq.(13)). Taking again the volume average of the last term, one obtains

$$\varphi_{,i} \simeq \hat{\varphi}_{,i} + \chi\,\tilde{\varphi}n_i \tag{20}$$

Thus, the Darcy's law can be expressed as

$$q_i = -k_{ij}\,\hat{\varphi}_{,j} = -k_{ij}\varphi_{,j} + k_{ij}\chi\tilde{\varphi}n_j \tag{21}$$

where q_i is the discharge per unit area and k_{ij} is the hydraulic conductivity operator. An impermeable interface/macrocrack can be defined by imposing the constraint $q_n = n_i q_i = 0$, so that

$$-n_i k_{ij}\,\varphi_{,j} + n_i k_{ij}\chi\tilde{\varphi}n_j = 0 \rightarrow \tilde{\varphi} = \frac{1}{\chi\, n_p k_{pq}\, n_q}\, n_i k_{ij}\,\varphi_{,j} \tag{22}$$

Substituting eq. (22) back into eq. (21), leads to a modified form of Darcy's relation, i.e.

$$q_i = -\tilde{k}_{ij}\,\phi_{,j} \quad \textit{where} \quad \tilde{k}_{ij} = k_{ij} - \frac{1}{n_p k_{pq} n_q}(k_{ik}n_k)(n_l k_{lj}) \tag{23}$$

where $\tilde{k}_{ij}$ is the equivalent hydraulic conductivity within a domain containing an impervious interface. Note that in this case, the formulation is independent of χ, which implies that there is no need to define the geometry of crack through the level-set method. Thus, the implementation of this approach within the standard FEM packages is quite straightforward.

3.2 Numerical example

In order to illustrate the approach outlined in Section 3.1, consider a constant head permeability set up in which a shale sample is subjected to a steady state flow under a prescribed hydraulic gradient. Given the material microstructure, the hydraulic properties are transversely isotropic with the preferred directions being associated with the bedding planes. Assume some typical values of hydraulic conductivity along those orientations, i.e. $k_2 = 1\times10^{-12}$ m/s, $k_1 = 4k_2$, where $1,2$ correspond to the normal and tangential direction, respectively. Geometry of the problem is shown in Fig.9. Two sets of simulations were conducted here, one by taking into account the randomly distributed sealed cracks shown in Fig.9, and the other one assuming an intact domain. For the elements containing the crack, the permeability operator was assigned according to eq.(23).

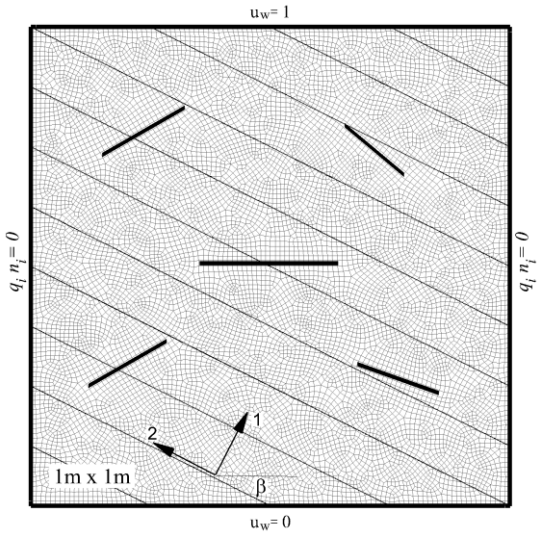

Figure 9- The flow domain (1m x 1m), with randomly distributed impermeable cracks, subjected to constant fluid pressure $u_w = 1$ MPa and $u_w = 0$ at the top and bottom, respectively

Fig.10 shows the stream lines superimposed on the distribution of pore water pressure in steady state conditions for both the cracked and the intact domain. Here, the vectors shown along the bottom boundaries are the discharge velocities scaled with respect to the magnitude of the maximum velocity. The results presented in this figure correspond to (a) isotropic conditions $k_1 = k_2$, (b) anisotropic case with $k_1 = 4k_2$ and horizontal bedding planes, i.e. $\beta = 0$, and (c) $k_1 = 4k_2$ and $\beta = 45°$. It is evident that the simple framework, viz. eq.(23), can efficiently reproduce the presence of impermeable interfaces. Fig.11 shows the resultant discharge velocity field, $q = \left(q_i\, q_i\right)^{1/2}$, for all previously mentioned scenarios. It should be noted that the flow pattern is consistent with the prescribed boundary conditions; also, the singular behaviour around the crack tips is adequately captured here.

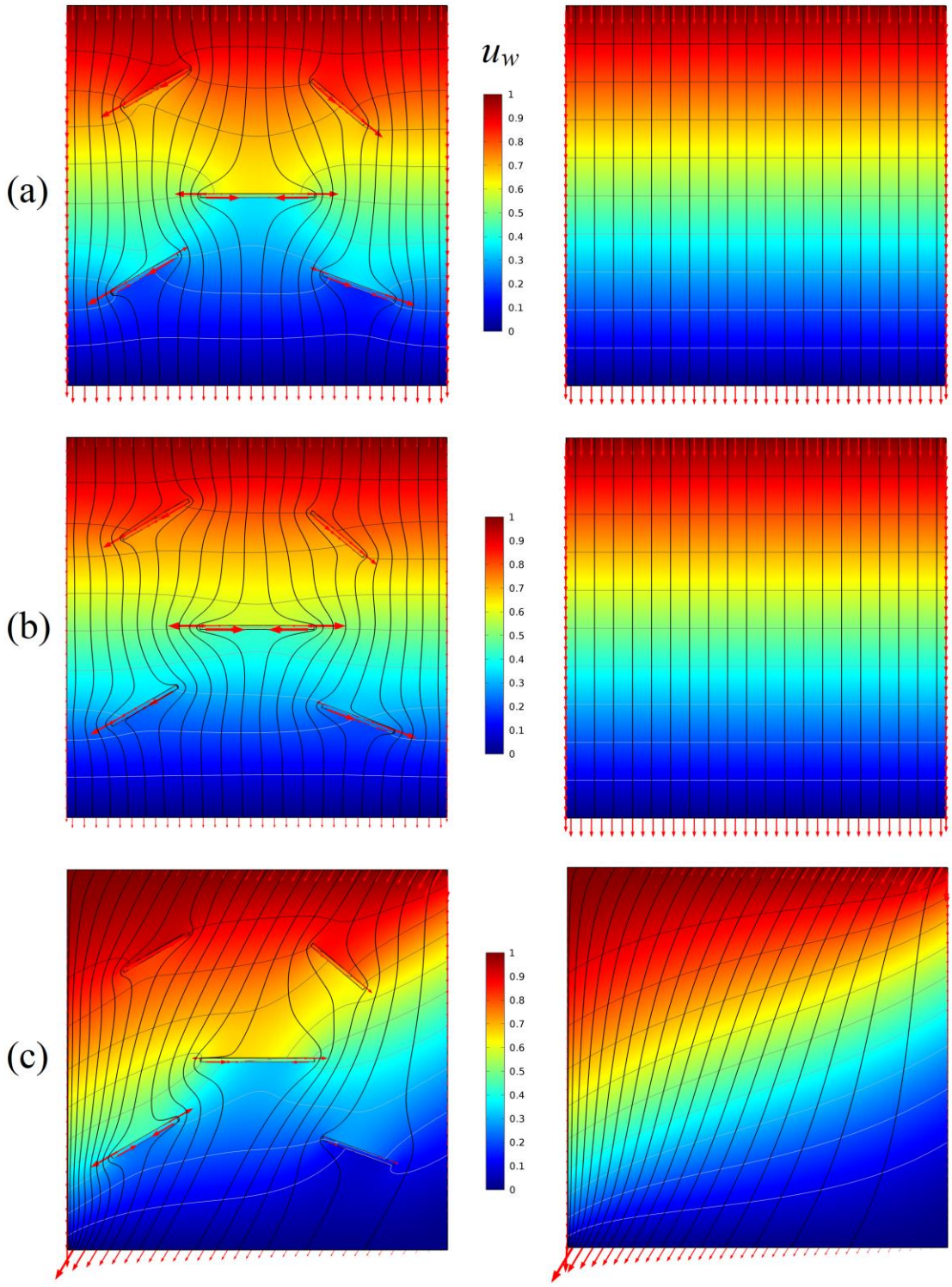

Figure 10- The stream lines superimposed on the contours of pore pressure distribution u_w (in MPa); a) isotropic case $k_1 = k_2$, b) anisotropic case with $k_1 = 4k_2$ and $\beta = 0^0$, c) anisotropic case with $k_1 = 4k_2$ and $\beta = 45^0$ (Left: w/cracks, Right: homogeneous domain)

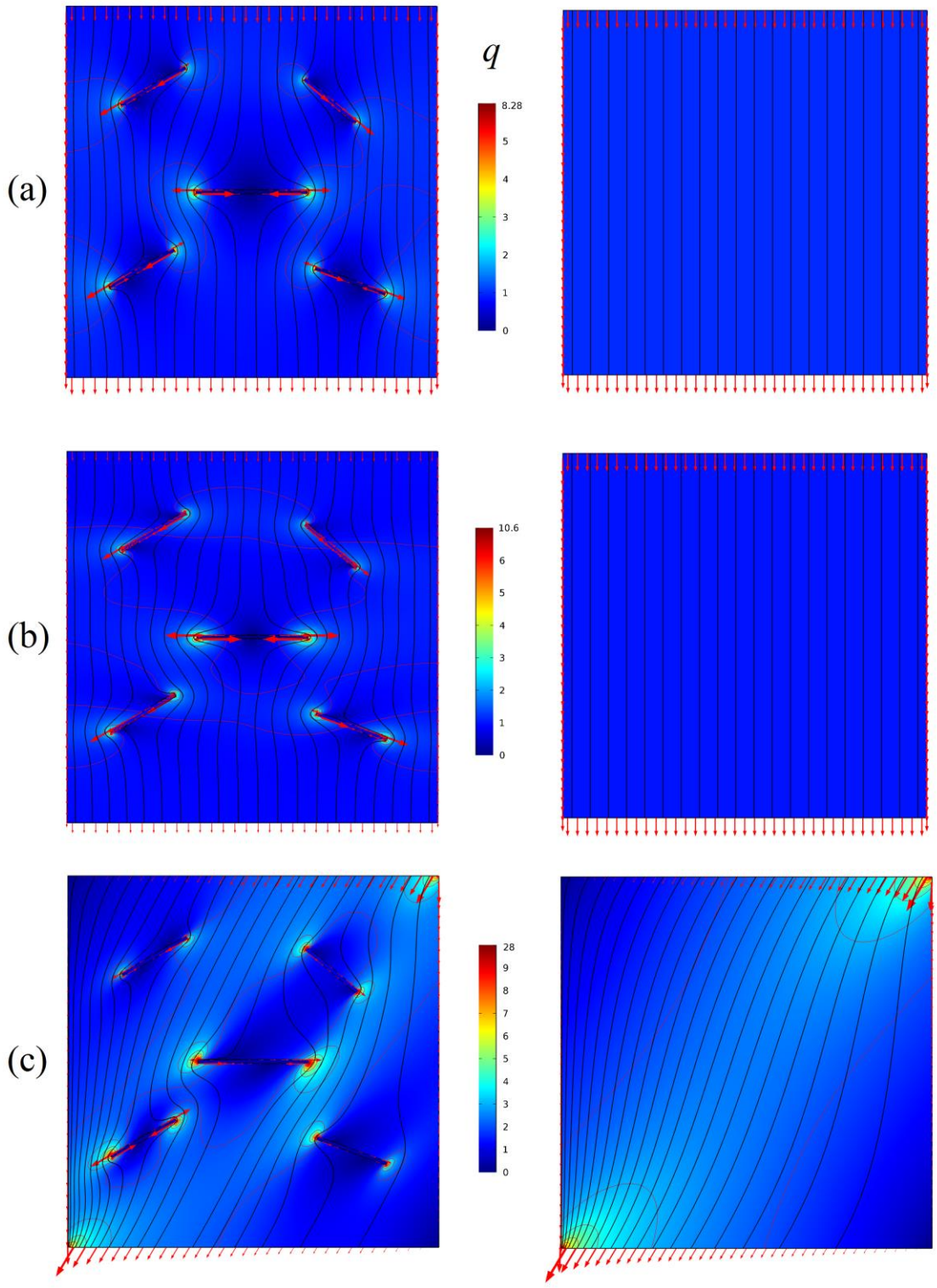

Figure 11- The stream lines superimposed on the contours of the discharge velocity magnitudes q (1×10^{-6} m/s); a) isotropic case $k_1 = k_2$, b) anisotropic case with $k_1 = 4k_2$ and $\beta = 0^0$, c) anisotropic case with $k_1 = 4k_2$ and $\beta = 45^0$ (Left: w/cracks, Right: homogeneous domain)

4. Final remarks

There is a broad scientific consensus that highly toxic nuclear waste is best disposed of deep underground. The feasibility of sedimentary rocks, in particular shale/clay, for the disposal concepts has been evaluated in a number of different countries and it has been assessed as a favourable medium for this purpose. With this in mind, the first part of this study dealt with presenting a methodology for an assessment of the long-term damage due to a deep excavation in a sedimentary rock. The approach incorporated the effect of inherent anisotropy in relation to both the specification of conditions at failure and description of the deformation process. For the latter, the instantaneous response as well as the time-dependent behaviour associated with chemo-mechanical interaction have been accounted for. The framework has also been combined with an embedded discontinuity approach to simulate the post-failure response involving the localized deformation. The methodology has been illustrated by a numerical example simulating the evolution of EDZ around a deep underground borehole. The assessment was mainly qualitative, as no adequate information was available on the selection of material parameters. However, the general conclusions pertaining to the extent and location of damage are consistent with the experimental observation.

The second part dealt with a modified form of Darcy's law for modeling the flow in the presence of impermeable discontinuities. The approach incorporated the enhanced embedded discontinuity model, conceptually similar to that used for the mechanical analysis of localized deformation. The flow pattern was examined for the case of a homogeneous flow domain as well as the case of a flow around a set of randomly distributed impervious macrocracks embedded within the flow region. The results show that the proposed strategy can accurately reproduce the local impermeability constraints, without any requirement for re-meshing. Thus, the approach is numerically quite efficient. The simulations shown are limited to the case of impervious discontinuities; however, the approach can be extended to permeable macrocracks as well.

REFERENCES

[1] Attewell PB, Sandford MR. Intrinsic shear strength of a brittle, anisotropic rock—I: Experimental and mechanical interpretation. Int. J. Rock Mech. Min. Sci. Geomech. Abstr., vol. 11, 1974, p. 423–30.

[2] Donath FA. Experimental study of shear failure in anisotropic rocks. Geol. Soc. Am. Bull. 1961;72:985. doi:10.1130/0016-7606(1961)72[985:ESOSFI]2.0.CO;2.

[3] Hoek E. Strength of jointed rock masses. Géotechnique 1983;33:187–223. doi:10.1680/geot.1983.33.3.187.

[4] Lérau J, Saint-Leu C, Sirieys P. Anisotropie de la dilatance des roches schisteuses. Rock Mech Felsmechanik Mec Des Roches 1981;13:185–96. doi:10.1007/BF01239037.

[5] Niandou H, Shao JF, Henry JP, Fourmaintraux D. Laboratory investigation of the mechanical behaviour of Tournemire shale. Int. J. Rock Mech. Min. Sci. 1997;34:3–16. doi:10.1016/S1365-1609(97)80029-9.

[6] Abdi H, Labrie D, Nguyen TS, Barnichon JD, Su G, Evgin E, et al. Laboratory investigation on the mechanical behaviour of Tournemire argillite. Can. Geotech. J. 2015;52:268–82. doi:10.1139/cgj-2013-0122.

[7] Yang M-T, Hsieh H-Y. Direct tensile behavior of a transversely isotropic rock. Int. J. Rock Mech. Min. Sci. 1997;34:837–49. doi:10.1016/S1365-1609(96)00065-4.

[8] Nova R, Zaninetti A. An investigation into the tensile behaviour of a schistose rock. Int. J. Rock Mech. Min. Sci. Geomech. Abstr. 1990;27:231–42. doi:10.1016/0148-9062(90)90526-8.

[9] Minh DN, Bergues J, Hoteit N, others. Determination of mechanical behaviour of claystones. 9th ISRM Congr., 1999.

[10] Naumann M, Hunsche U, Schulze O. Experimental investigations on anisotropy in dilatancy, failure and creep of Opalinus Clay. Phys. Chem. Earth., Parts A/B/C 2007;32:889–95. doi:10.1016/j.pce.2005.04.006.

[11] Duveau G, Shao JF, Henry JP. Assessment of some failure criteria for strongly anisotropic geomaterials. Mech. Cohesive-Frictional Mater. 1998;3:1–26.

[12] Kwasniewski MA. Mechanical behavior of anisotropic rocks. Compr. Rock. Eng. 1993;1:285–312.

[13] Pietruszczak S, Haghighat E. Modeling of deformation and localized failure in anisotropic rocks. Int. J. Solids. Struct. 2015.

[14] Pietruszczak S, Lydzba D, Shao JF. Description of creep in inherently anisotropic frictional materials. J. Eng. Mech. 2004;130:681–90. doi:10.1061/(ASCE)0733-9399(2004)130:6(681).

[15] Haghighat E, Pietruszczak S. On modeling of discrete propagation of localized damage in cohesive-frictional materials. Int. J. Numer. Anal. Methods. Geomech. 2015:n/a – n/a. doi:10.1002/nag.2368.

[16] Pietruszczak S, Mróz Z. Finite element analysis of deformation of strain-softening materials. Int. J. Numer. Methods Eng. 1981;17:327–34. doi:10.1002/nme.1620170303.

[17] Haghighat E, Pietruszczak S, Su G, Nguyen TS. Numerical investigation of the mechanical behaviour of Tournemire argillite. ISRM Congr., Montreal: 2015.

[18] Lisjak A, Grasselli G, Vietor T. Continuum–discontinuum analysis of failure mechanisms around unsupported circular excavations in anisotropic clay shales. Int. J. Rock Mech. Min. Sci. 2014;65:96–115. doi:10.1016/j.ijrmms.2013.10.006.

[19] Bock H. RA Experiment. Updated review of the rock mechanics properties of the Opalinus Clay of the Mont Terri URL based on laboratory and field testing. 2009.

[20] Pietruszczak S. Fundamentals of plasticity in geomechanics 2010.

[21] Haghighat E, Pietruszczak S. On modeling of cracks using the enhanced embedded discontinuity method. Manuscript Submitted for Publication 2015.